Temporal, probabilistic mapping of ash clouds using wind field stochastic variability and uncertain eruption source parameters: Example of the 14 April 2010 Eyjafjallajökull eruption

E.R. Stefanescu,[1] A.K. Patra,[1] M.I. Bursik,[2] R. Madankan,[1] S. Pouget,[2] M. Jones,[3] P. Singla,[1] T. Singh,[1] E.B. Pitman,[4] M. Pavolonis,[5] D. Morton,[6] P. Webley[6], and J. Dehn[6]

Abstract. In a previous contribution, we analyzed the probability of ash presence using weighted samples of volcanic ash transport and dispersal model runs and a reanalysis wind field to propagate uncertainty in eruption source parameters. In this contribution, the probabilistic modeling is extended by using ensemble forecast wind fields as well as uncertain source parameters. The impact on ash transport of variability in wind fields due to unresolved scales of motion as well as model physics uncertainty is also explored. We have therefore generated a probabilistic forecast of volcanic ash transport with only a priori information, quantifying and exploring uncertainty in both wind and the volcanic source.

1. Introduction

Volcano observatories and volcanic ash advisory centers (VAACs) predict the likely position of ash clouds generated by explosive volcanic eruptions using deterministic mathematical models of advection and dispersion, known as volcanic ash transport and dispersal (VATD) models [*Langmann et al.*, 2012; *Folch*, 2012]. These models require input data on volcanic source conditions as well as the wind field [*Mastin et al.*, 2009]. The resulting maps are often understood to delineate "hard" exclusion zones. In contrast, most meteorological forecasts are issued as maps or reports giving the probability of an event or the occurrence of a phenomenon, like precipitation, in a certain region at a specific time [*Zhang and Krishnamurti*, 1999]. Partly because of this disparity between ash cloud and meteorological forecasting, and the desire to produce ash forecast products comparable to the standard, a need has been expressed on numerous occasions for probabilistic ash cloud forecasts [*IVATF*, 2011].

In previous work [*Bursik et al.*, 2012], we analyzed the probability of ash presence using a VATD and a reanalysis wind field, which is only available a posteriori, to propagate uncertainty in volcanic eruption source parameters. In this contribution, we extend the previous work by using ensemble forecast wind fields, and explore the impact of variability in wind fields due to unresolved scales and uncertain model physics, *i.e., we construct and evaluate a probabilistic forecast with only a priori information, which accounts for uncertainty in both wind and the volcanic source.* In developing a complete probabilistic forecast for ash location with time, we thus investigate the effects of aleatoric uncertainty associated with volcanic eruption source parameters and the wind field using suitable ensembles, and epistemic uncertainty associated with the advective equations of motion by investigating outputs of both multi-model and spectral ensembles.

Bursik et al. [2012] began the process of uncertainty estimation and probabilistic ash cloud forecasting by addressing the problem of propagation of uncertainties in the volcanic input parameters to produce a coherent probabilistic forecast of ash cloud position. Fully probabilistic output of ash transport and dispersion models depends on uncertainty in winds as well as uncertainty in the input eruption source parameters. Therefore, to fully implement probabilistic modeling, we couple three numerical tools: 1) the Weather Research and Forecast (WRF) model is used to forecast an uncertain wind field based on boundary conditions provided by the GEFS ensemble, 2) a volcanic eruption column model, `bent` [*Bursik*, 2001], is employed to incorporate eruption observations and characterize source parameter uncertainty. Samples from the random variables in source parameter space of `bent` were drawn using the Conjugate Unscented Transform (CUT) [*Adurthi et al.*, 2012]. These uncertain source parameters are then propagated to outputs suitable to provide initial conditions for 3) a VATD model, `PUFF` [*Searcy et al.*, 1998], which is used to propagate ash parcels in the uncertain wind field.

The results of probabilistic forecasts are tested with standard methods against satellite data for the paroxysmal phase of the Eyjafjallajokull eruption of 14–18 April, 2010. We furthermore test the GEFS ensemble method, qualitatively evaluating the effects of different physics by comparing the spread in certain multi-model ensemble outputs with those of the GEFS ensemble at specified locations. Finally, output based on the SKEB scheme is employed to investigate the potential effects of unresolved scales in atmospheric motion on ash cloud spread.

2. Background

Measures of eruption intensity and grain size represent some of the major sources for uncertainty in ash transport and dispersion simulations [*Mastin et al.*, 2009; *Dacre et al.*, 2011; *Bursik et al.*, 2012; *Webley et al.*, 2012]. Estimates of the magnitude of the uncertainty are also needed. Because of our lack of knowledge of the exact conditions at

[1]Department of Mechanical and Aerospace Engineering, University at Buffalo, Buffalo, New York, USA.
[2]Department of Geology, University at Buffalo
[3]Center for Computational Research, University at Buffalo
[4]Department of Mathematics, University at Buffalo
[5]NOAA-NESDIS Center for Satellite Applications and Research, Madison, WI, USA.
[6]Geophysical Institute, University of Alaska, Fairbanks, USA.

0148-0227/14/$9.00

the volcanic source at the time of an eruption, probability distributions are assigned to the eruption source parameters based on samples of past eruptions which have been collected from the historical record, or real-time data that lend some insight into current eruption conditions. We sample the probability density functions using a non-Monte Carlo technique that optimizes moment calculations. In this contribution, simulation ensembles with different input volcanic source parameters are intelligently chosen to predict the average and higher order moments of the output correctly.

Ensemble modeling, originally developed for weather prediction, is being extended to atmospheric dispersion applications [*Krishnamurti et al.*, 2000; *Galmarini et al.*, 2004]. Several techniques have been developed over the last decade for the ensemble treatment of atmospheric dispersion model predictions. Among them, two have received most of the attention — the multi-model and the ensemble prediction system (EPS) model [*Potempski et al.*, 2008; *Galmarini et al.*, 2010]. The multi-model approach relies on model simulations produced by different atmospheric dispersion models using meteorological data from potentially different weather prediction systems. The EPS-based ensemble is generated by running a single atmospheric dispersion model with ensemble weather prediction members.

The use of dispersion fields produced using different meteorological fields is particularly suitable when the latter are forecast fields for which no measurements are available for model validation and tuning. The multi-circulation, multi-dispersion model ensemble allows the analysis of a wide spectrum of scenarios resulting from different numerical weather prediction (NWP) simulations and approaches to dispersion modeling. Furthermore, ensemble analysis turns out to be an efficient method to obtain probabilistic results, which are useful for estimating the sensitivity of the simulation to initial conditions, physics described by the models, algorithm implementation, numerics, representation of surface properties, boundary conditions, source term description and source representation.

For the atmospheric characterization incorporated into a dispersion model, an ensemble prediction is a feasible way to extend a single, deterministic forecast with an estimate of the probability density function of forecast weather states [*Warner*, 2011; *Galmarini et al.*, 2004]. There are methods to generate initial condition uncertainty in wind ensembles and produce perturbations that have dynamically consistent structures. At the National Centers for Environmental Prediction (NCEP), *Toth and Kalnay* [1993] introduced the bred–vector (BV) perturbation method to create the Global Ensemble Forecast System (GEFS) wind field forecast. Here, we use the NCEP GEFS ensemble to initialize a Numerical Weather Prediction (NWP) model, used in a forecast mode, and couple that with our uncertainty model of eruption source parameter to produce a complete model of the uncertainty in the ash cloud forecast.

The model created by propagating both wind field uncertainty through the GEFS ensemble and eruption source parameter uncertainty does not account for lack of sometimes properly characterizing the physics of the atmosphere [*Potempski et al.*, 2008]. Using a multi-model ensemble, one aims to capture the model-related forecast uncertainty by averaging the individual physics members using equal weights. A more rational method for combining the model solutions was proposed by *Raftery et al.* [1997], which “rewards” better physical characterization by weighting.

Due to finite model resolution, the physical processes that span numerous orders of magnitude of spatial scales must be approximated (parametrized). Recently, stochastic parametrization techniques have been applied to capture unresolved or poorly represented scales of motion in such a way that the models have a statistical or spectral behavior that is consistent with observations of the entire atmosphere. The stochastic kinetic-energy backscatter (SKEB) scheme [*Shutts*, 2005] is one such method to generate a model that is spectrally consistent with the real atmosphere.

3. Methodology

3.1. WRF - `bent` - `PUFF` coupling

Because of the separate spatial scales and physics, eruption column (volcanic plume) models have generally been developed separately from VATD models. One such eruption column model, `bent` solves a cross-sectionally averaged system of equations for continuity, momentum and energy balance. It takes a size distribution of pyroclasts, then outputs the height distribution of the clasts in the atmosphere [*Bursik*, 2001]. In producing its eruption outputs, `bent` accounts for atmospheric (wind, temperature, pressure, etc.) conditions as given by atmospheric sounding or NWP data. It has been tested against plume rise height data, and against dispersal data [*Bursik et al.*, 2009]. Details of the volcanic source parameters along with assumptions and probability distributions used are presented in [*Bursik et al.*, 2012; *Madankan et al.*, 2013]. `bent` simulations output a volume into which particles are placed in the atmosphere around the volcano. These are released into the WRF gridded wind field, and their movement is calculated via the Lagrangian advection/diffusion model `PUFF`.

Given an initial ash-laden volume produced by `bent`, the `puff` Lagrangian VATD model was used to populate the volume, then propagate ash parcels in ensemble wind fields [*Searcy et al.*, 1998]. `puff` tracks a finite number of Lagrangian point particles of different sizes, whose location R is propagated from timestep k to timestep $k+1$ via an advection/diffusion equation

$$R_i(t_{k+1}) = R_i(t_k) + W(t_k)\Delta t + Z(t_k)\Delta t + S_i(t_k)\Delta t \quad (1)$$

Here $R_i(t_k)$ is the position vector of the i^{th} particle at time $k\Delta t$, $W(t_k)$ is the local wind velocity at the location of the i^{th} particle, $Z(t_k)$ is a turbulent diffusion that is modeled as a random walk, and $S_i(t_k)$ is a source term that models the fallout of the i^{th} particle due to gravity. Note therefore that `puff` takes into account dry particle fallout, as well as dispersion and advection.

To implement the WRF–`bent`–`PUFF` coupling, we consider a variable of interest (e.g. ash concentration at a location). We assume this to be a random variable, $\mathbf{x}_k$, whose time evolution is given by WRF-`bent-PUFF`:

$$\dot{\mathbf{x}} = \mathbf{f}(t, \mathbf{x}, \mathbf{\Theta}, \mathcal{W}) \quad (2)$$

In Eq 5, $\mathbf{\Theta} = \{\theta_1, \theta_2, ...\}$ represents uncertain system parameters such as the vent radius, eruption velocity, mean grain size and grain size variance and $\mathcal{W}$ is a given wind field from a NWP model.

Samples from the random variables in eruption source parameter space are drawn using the Conjugate Unscented Transform (CUT) [*Adurthi et al.*, 2012; *Madankan et al.*, 2013], and are then combined in a tensor-product fashion with each wind ensemble member. The main idea of the CUT approach is to select specific structures for symmetric points, rather than taking a tensor product of 1-D points as in the Gauss quadrature scheme. As a result, the quadrature points still exactly integrate polynomials of total degree $2N-1$ in n-dimensional space, while the number of points is much less than N^n. Here N represents the number of quadrature points needed to solve a one-dimensional integral (according to the Gaussian quadrature scheme).

The probability of having airborne ash at a specific height is given by:

$$P(h) = \int_\Omega P(h|W)p(W)dW \approx \frac{1}{N_W}\sum_{i=1}^{N_W} P(h|W_i) \quad (3)$$

while the expected value of height is:

$$E[h] = \int_{\Omega} hP(h)dh = \int_{\Omega_W} h(\theta, W) \left(\int_{\Omega_S} P(h|W)p(W)dW \right) dh \tag{4}$$

$$= \int_{\Omega_W} \int_{\Omega_S} h(\theta, W)P(h|W)p(W)dWdh$$

$$= \sum_{i=1}^{N_W} w_i \sum_{q=1}^{N_{CUT}} w_q h(\theta_q, W_i)$$

where w_i are the weights associated with the wind ensemble, while w_q are those for the eruption source parameters obtained from using a generalized polynomial chaos (gPC) expansion [*Bursik et al.*, 2012]. Ω_W and Ω_S are the wind field parameter space and eruption source term parameter space, respectively.

3.2. GEFS ensemble forecast

Major factors that influence the accuracy of NWP models are the resolution of the grid, uncertainty in the initial observations, and the use of different parameterization schemes. For wind fields, ensemble methods are considered to be an effective way to estimate the probability density function [*Mann*, 1998] of future states of the atmosphere by addressing uncertainties present in initial conditions and in model approximations. Ensemble forecasting provides human forecasters with a range of possible solutions, whose average is generally more accurate than the single deterministic forecast [*Kalnay*, 2003], and whose spread provides a quantitative basis for probabilistic forecasting. In terms of dispersion modeling, ensemble forecasting becomes more important when the dispersion simulations are forecasts for which there are sparse satellite data for validation, and when the model results are used for decision support or regulatory purposes [*Galmarini et al.*, 2010]. To construct the ensemble ash forecast then, uutput statistics of the volcanic ash location and three-dimensional ash concentrations are computed by properly summing the weighted values of the output parameters of interest.

For the Eyjafjallajökull eruptive events of April 2010, we use the 21 member NCEP "high resolution" GEFS forecasts produced four times daily [*Toth and Kalnay*, 1993] starting 0006 UTC April 16 to 0000 UTC April 18 on a 1° latitude by 1° longitude grid to investigate . For the time period of 0000 UTC April 14 to 0000 UTC April 16, we use NCEP/NCAR Reanalysis data as a deterministic realization of the wind fields as input to the VATD model. To generate high-resolution forecast wind fields from GEFS, the Weather Research and Forecasting – Advanced Research WRF (WRF–ARW) numerical weather prediction system [*Skamarock et al.*, 2005; *UCAR*, 2012] is used to interpolate GEFS outputs. The main physical options used in WRF include Kessler microphysics, Mellor-Yamada-Janjic planetary boundary layer (PBL) scheme [*Noh et al.*, 2003], and the Noah land surface model [*Chen and Dudhia*, 2001]. For each GEFS member forecast, a continuous WRF run/integration with a single GEFS initialization is done, resulting in outputs every 3 h at 74 pressure levels. The model domain is organized around the location of the Eyjafjallajökull vent (63.63°N and 19.63°S) with dimensions of 230 × 230 horizontal grid points at a spacing of 27 km, with 29 pressure levels (1000-100 hPa, excluding the surface), and comprises most of Europe.

3.3. Multi-model ensemble forecast

To understand the effects of the paucity of information (epistemic uncertainty) about which physics approaches to use in WRF, we tested WRF by comparing results from ensemble runs having different physics options (Table 1). Specifically, we tested if different WRF physics options were important in light of the uncertainty generated by GEFS by comparing multi-model and GEFS outputs with radiosonde data. We decided, a priori, that the approach (multi-model or GEFS) yielding the greatest variance in the wind field prediction would be the one to be used in the simulations, as it would presumably yield the greatest dispersion of ash cloud probability.

In theory, both ensembles can be used simultaneously, and in fact even more ensembles can be formed by using multi-model dispersion simulations [**?**]. However, the determination of the weights for the different members of such ensembles of ensembles is beyond the purview of the present contribution. We have therefore performed a simple test consisting of checking wind direction and amplitude forecasts from the two ensemble techniques with radiosonde data [*UWYO*, 2012] at two locations along the path of the ash towards Europe (Lerwick, Shetland Islands, at 60.13° N and 1.18° W, and Praha-Libus, Czech Republic, at 50.00° N and 14.45° E) (Fig. 1). We chose to compare with radiosonde data since wind velocity is no doubt the most important control on ash cloud motion. Multi-model (see Table 1 for the physics options) ensembles sometimes generated dramatically less variability in forecast wind fields than did GEFS initial condition ensembles (Fig. 1). This result suggested that in the present case the GEFS ensemble is a better choice to most fully capture wind field variability to be used in calculating probabilistic ash hazards maps. This result is consistent with previous comparisons of the effects of multi-model and initial-condition ensembles on dispersion forecasts [*Galmarini et al.*, 2010].

3.4. Stochastic kinetic-energy backscatter (SKEB)

Forward time integration is performed using numerical models designed to simulate different physical processes in the atmosphere. These processes are active at scales smaller than the grid size used in the numerical integration, and thus remain unresolved and can only be approximated [*Buizza and Palmer*, 1995; *Shutts*, 2005; *Berner et al.*, 2008]. This misrepresentation of unresolved subgrid-scale processes is deemed to be model error, and may be addressed by introducing a stochastic element into atmospheric models by randomly perturbing the increments or tendencies from parameterization schemes [*Buizza et al.*, 1999; *Palmer et al.*, 2009]. Other approaches seek to formulate the parameterization schemes in a stochastic way [*Palmer and Williams*, 2008; *Plant and Craig*, 2008]. Here, we explore the potential effects of the unresolved sub-grid scale processes by using a stochastic kinetic energy backscatter (SKEB) algorithm [*Shutts*, 2005, 2008], which is a simplified version of the algorithm of *Berner et al.* [2009]. The SKEB scheme is based on the notion that the turbulent dissipation rate is a function of the difference between upscale and downscale spectral kinetic energy transfer [*Shutts*, 2005]. The scheme implemented here assumes a spatially and temporally constant dissipation rate.

The stochastic perturbation fields for wind and temperature are controlled by the kinetic and potential energy they inject into the flow. The injected energy is expressed as a backscattered dissipation rate for the streamfunction and temperature, respectively. To investigate the potential variability introduced by our lack of properly characterizing the spectral characteristics of the atmospheric motion with SKEB, WRF simulations were performed for the same time period, and same initial conditions and physics options, as described above for the Eyjafjallajökull eruption with SKEB option ON and OFF. We then visualized the variability by comparing ash cloud positions and shapes.

3.5. Construction of probabilistic maps

To produce the probabilistic forecast, we thus used each GEFS ensemble member as WRF input, keeping physics and dynamics options the same for all runs. The ensemble wind field was then constructed from the high-resolution WRF models, each of which used a separate GEFS ensemble member for boundary conditions. Samples from the random variables of eruption velocity, vent radius, mean grain size and grain size standard deviation in eruption source parameter space were drawn using the CUT method, and were then combined in a tensor-product fashion with each wind ensemble. Use of the CUT method results in 161 quadrature points (for 4 dimensions of uncertain input eruption source parameters), combined with a 21-member wind ensemble, leading to 3381 simulation runs.

Following runs of `bent` at the CUT sample points, each `bent` output was then propagated through `PUFF`, for each WRF ensemble member. The outputs from `PUFF` were then combined by applying the appropriate weight to each deterministic WRF-`bent-PUFF` run. The result is a map of the probability of having airborne ash at a point, which is compared with satellite images (Fig. 2). At present, examination of satellite data provides the best quantitative method for detecting and analyzing ash clouds.

4. Results and discussion

In this contribution, we forecast ash cloud movement by treating the wind as a random variable along with the volcanic input parameters of vent radius, vent velocity, mean grain size and grain size variance. To discuss uncertainty and its effects on models, we distinguish between parametric uncertainty and wind field forcing uncertainty. Methodologically, these two kinds of uncertainty are accounted for differently. In a deterministic setting, ash concentration at a given time and location is based on integration of advected `PUFF` particles. In developing a probabilistic forecast for the ash location, we treat the model outputs at a given location and time as random variables, and the appropriate output from each "run" of the WRF–`bent`–`PUFF` simulation is a sample from that random variable.

The procedure used to calculate the probability of the presence of ash in the atmosphere was introduced in [*Bursik et al.*, 2012] and is extended here to account for the new uncertainty in the wind field. Consider a variable of interest (e.g. ash cloud top height at a location). We assume this to be a random variable, $\mathbf{x}_k$, whose time evolution is given by the WRF-`bent-PUFF` coupled eruption column advection/diffusion solver, written generically as:

$$\dot{\mathbf{x}} = \mathbf{f}(t, \mathbf{x}, \boldsymbol{\Theta}, \mathcal{W}) \tag{5}$$

In Eq 5, $\boldsymbol{\Theta} = \{\theta_1, \theta_2, ...\}$ represents uncertain system parameters such as the vent radius, vent velocity, mean grain size and grain size variance and $\mathcal{W}$ is a given wind field from the GEFS–WRF NWP model.

The effect of the uncertainty in the wind field on the forecast has been evaluated by standard meteorological measures of error and goodness-of-fit. In the case of the combined WRF–`bent`–`PUFF` runs, we have evaluated the statistical properties of the ensemble forecasts using two measures that can be applied in cases where a probabilistic meteorological forecast is being tested against binary observations, in our case the presence or absence of an ash cloud in SEVIRI data (see [*Bursik et al.*, 2012]. Because of the difficulty of using the data from any one instrument to determine the position of all airborne ash, the results must be understood relative one to another rather than in an absolute sense. Nevertheless, there is reason to believe that SEVIRI provides the best estimate of airborne ash from any single instrument available for the eruption under consideration.

In previous work [*Bursik et al.*, 2012], we constructed a probability map of airborne ash when accounting only for eruption source parameter uncertainty. In the present contribution, we additionally explore the nature of the contribution of wind field uncertainty. Qualitative snapshots comparing the performance of models with and without wind field uncertainty are shown in Figure 2. It can be observed that probability maps for both reanalysis (colored regions in Figure 2) and GEFS models rather thoroughly cover the region where volcanic ash exists according to satellite imagery (black regions), given a 24-h wind field forecast (black lines in Figure 2). The match between model and data is much worse when using a 60-h wind field forecast (red lines in Figure 2), as would be expected.

We can evaluate the comparisons between model and data in a quantitative fashion by using the Brier Score. The Brier Score in the present context is the mean squared difference between the probability of ash assigned by the forecast to a particular position, and the absence (= 0) or presence (= 1) of ash in the SEVIRI image. The Brier score calculated from the use of reanalysis data is equal to 0.3225, while for the GEFS 24-h forecast data, it is 0.2048. Thus, even though use of the GEFS ensemble introduces more variability, the error in the forecast actually decreases, as the ensemble produces a 24-h forecast that better matches SEVIRI data than does the use of reanalysis data. This must mean, enigmatically and perhaps serendipitously, that the GEFS ensemble forecast better represents the true wind field than does the reanalysis. We believe that this result must arise from the fact that within a data assimilation cycle, the higher spatial resolution WRF model used with GEFS provides a better estimate of the wind field than does reanalysis data.

We have used the ROC curve to further explore the difference between the use of reanalysis and GEFS forecast data. The ROC curve is usually used to provide information on the hit and false alarm rates that are obtained by probabilistic output. In our case, we used the ROC curve to compare output using the GEFS ensemble and eruption source parameter uncertainty as a continuous probability, with output using reanalysis data and eruption source parameter uncertainty reduced to a binary presence or absence of ash. A cell was defined to contain ash if the absolute concentration exceeded 10^{-10} mg/m^3 Hit and false alarm rates were plotted using a probability threshold of 10% (Fig. 3). The vertical axis gives the hit rate, defined as the number of times the event was forecast (uncertain source parameters and ensemble wind fields both used) and later observed (source parameters only used) to occur. The area under the ROC curve is often used as a single summary measure. A larger area is better (a perfect forecast has area = 1). When we compare the area under the curve for the two forecasts, for the one started at 0000 UTC April 16 we get a better approximation of the footprint (area = 0.903), than the one started at 0000 UTC April 14 (area = 0.622). This finding is consistent with the Breier Score. The ROC score indicates that relatively good prediction skill.

We have already touched upon the effects of the multi-model approach in our evaluation of the forecast radiosondes (Fig. 1), which seemed to generally introduce less variability than GEFS into the wind field. We therefore did not pursue any `PUFF` runs with the multi-model ensemble. However, to explore the potential effects of greater uncertainty in ash cloud position resulting from unresolved, short wavelength scales of wind field motion (related to "underdispersiveness" in NWP ensembles ; *Berner et al.* [2009]), WRF simulations were performed using the SKEB scheme, with realizations of PUFF being run with SKEB on or off and the outputs compared (Fig. 4). The results suggest that SKEB indeed causes greater ash cloud dispersion, apparently by increasing scatter in vorticity and energy at length scales of hundreds of km. The result on ash dispersion as shown by comparing PUFF runs is primarily to increase the stretching mode of the ash cloud more than the bending and diffusion modes as defined by *Bursik* [1998]. Although application of SKEB does therefore result in an ensemble ash cloud of greater extent, the ensemble still contains insufficient variability to encompass the observed ash cloud given a 60 h forecast. This may be because SKEB does not introduce significant variability at the synoptic scale.

5. Conclusions

For the first time, volcanic ash cloud simulation results are presented as probabilistic envelopes showing the effects of volcanic source term uncertainty and wind field stochastic variability on a forecast. We tested the reliability of the forecast using standard meteorology metrics. The results suggest that standard ensemble or probabilistic forecasting can yield reasonable, usable results given < 24 h forecasts, without resorting to source-parameter inversion, Bayesian updating or Kalman filtering [*Stohl et al.*, 2011]. These methodologies can, however, improve the details of the local footprint of the forecast model relative to later satellite data acquisitions [*Madankan et al.*, 2012]. Forecasts several days downstream (to 60 h) could not at this time be improved by any available ensembling technique to provide sufficient long-wavelength dispersion to allow for a probabilistic forecast envelope to encompass known position of ash.

In the future, we seek to integrate improved estimates of mass eruption rate and mass loading [*Pouget et al.*, 2013], as well as source parameter inversion or Bayesian updating, as appropriate [*Madankan et al.*, 2013]. The first would perhaps make possible reasonable estimation of mass loading and concentration, and the latter better estimation of the short-wavelength footprint.

Acknowledgments. We thank Judith Berner for useful discussions regarding this work. The work reported herein was supported by AFOSR contract number FA9550-11-1-0336, and by NSF CMMI-1131074. All results and opinions expressed in this article are those of the authors and do not reflect opinions of NSF or 484 AFOSR.

References

Adurthi, N., P. Singla, and T. Singh (2012), The Conjugate Unscented Transform – an approach to evaluate multidimensional expectation integrals, in *American Control Conference (ACC), 2012*, pp. 5556–5561, IEEE.

Adurthi, A. (2012), A review of tephra transport and dispersal models: Evolution, current status, and future perspectives, in *Journal of Volcanology and Geothermal Research*, *235-236*, 5556–5561.

Berner, J., F. Doblas-Reyes, T. Palmer, G. Shutts, and A. Weisheimer (2008), Impact of a quasi-stochastic cellular automaton backscatter scheme on the systematic error and seasonal prediction skill of a global climate model, *Philosophical Transactions of the Royal Society A: Mathematical, Physical and Engineering Sciences*, *366*(1875), 2559–2577.

Berner, J., G. Shutts, M. Leutbecher, and T. Palmer (2009), A spectral stochastic kinetic energy backscatter scheme and its impact on flow-dependent predictability in the ecmwf ensemble prediction system, *Journal of the Atmospheric Sciences*, *66*(3), 603–626.

Buizza, R., and T. Palmer (1995), The singular-vector structure of the atmospheric global circulation, *Journal of the Atmospheric Sciences*, *52*(9), 1434–1456.

Buizza, R., M. Milleer, and T. Palmer (1999), Stochastic representation of model uncertainties in the ecmwf ensemble prediction system, *Quarterly Journal of the Royal Meteorological Society*, *125*(560), 2887–2908.

Bursik, M. (2001), Effect of wind on the rise height of volcanic plumes, *Geophys. Res. Lett.*, *18*, 3621–3624.

Bursik, M., S. Kobs, A. Burns, O. Braitseva, L. Bazanova, I. Melekestsev, A. Kurbatov, and D. Pieri (2009), Volcanic plumes and the wind: jetstream interaction examples and implications for air traffic, *J. of Volcanology and Geothermal Research*, *186*, 60–67.

Bursik, M., M. Jones, C. Carn, K. Dean, A. Patra, M. Pavolonis, E. Pitman, T. Singh, P. Singla, P. Webley, H. Bjornsson, and M. Ripepe (2012), Estimation and propagation of volcanic source parameter uncertainty in an ash transport and dispersal model: application to the Eyjafjallajokull plume of 14 - 16 April 2010, *Bull Volcanol*, *74*, 2321–2338.

Chen, F., and J. Dudhia (2001), Coupling and advanced land surface-hydrology model with the Penn State-NCAR MM5 modeling system. Part I: Model implementation and sensitivity, *Mon. Weather Rev.*, *129*, 569–585.

Dacre, H., A. Grant, R. Hogan, S. Belcher, D. Thomson, B. Devenish, F. Marenco, M. Hort, J. M. Haywood, A. Ansmann, et al. (2011), Evaluating the structure and magnitude of the ash plume during the initial phase of the 2010 Eyjafjallajökull eruption using lidar observations and NAME simulations, *Journal of Geophysical Research: Atmospheres (1984–2012)*, *116*(D14).

Galmarini, S., R. Bianconi, W. Klug, T. Mikkelsen, R. Addis, S. Andronopoulos, P. Astrup, A. Baklanov, J. Bartniki, J. Bartzis, et al., Ensemble dispersion forecastingpart i: concept, approach and indicators, *Atmospheric Environment*, *38*(28), 4607–4617, 2004.

Galmarini, S., F. Bonnardot, A. Jones, S. Potempski, L. Robertson, and M. Martet, Multi-model vs. eps-based ensemble atmospheric dispersion simulations: A quantitative assessment on the etex-1 tracer experiment case, *Atmospheric Environment*, *44*(29), 3558–3567, 2010.

Gilbert, J., and R. Sparks (1998), Tephra dispersal. the Physics of Explosive Volcanic Eruptions, *Geological Society of London Special Publication*, *145*, 115144.

Gudmundsson, M. T., T. Thordarson, Á. Höskuldsson, G. Larsen, H. Björnsson, F. J. Prata, B. Oddsson, E. Magnússon, T. Högnadóttir, G. N. Petersen, et al. (2012), Ash generation and distribution from the April-May 2010 eruption of Eyjafjallajökull, Iceland, *Scientific reports*, *2*. xx

IVATF (2011), International Volcanic Ash Task Force (IVATF) - Second Meeting, `http://www.icao.int/safety/meteorology/ivatf/Meeting%20MetaData/IVATF.2.WP.012.2.en.pdf`.

Kalnay, E. (2003), *Atmospheric modeling, data assimilation, and predictability*, Cambridge university press.

Langmann, B., A. Folch, M. Hensch, and V. Matthias (2012), Volcanic ash over Europe during the eruption of Eyjafjallajökull on iceland, April–May 2010, *Atmospheric Environment*, *48*, 1–8.

Krishnamurti, T. N., C. Kishtawal, Z. Zhang, T. LaRow, D. Bachiochi, E. Williford, S. Gadgil, and S. Surendran, Multimodel ensemble forecasts for weather and seasonal climate, *Journal of Climate*, *13*(23), 4196–4216, 2000.

Madankan, R., P. Singla, A. Patra, M. Bursik, J. Dehn, M. Jones, M. Pavolonis, B. Pitman, T. Singh, and P. Webley, Polynomial chaos quadrature-based minimum variance approach for source parameters estimation, *Procedia Computer Science*, *9*, 1129–1138, 2012.

Madankan, R., S. Pouget, P. Singla, M. Bursik, J. Dehn, M. Jones, A. Patra, M. Pavolonis, E. Pitman, T. Singh, et al., Computation of probabilistic hazard maps and source parameter estimation for volcanic ash transport and dispersion, *Journal of Computational Physics*, 2013.

Mann, J. (1998), Wind field simulation, *Probabilistic engineering mechanics*, *13*(4), 269–282.

Mastin, L., M. Guffanti, R. Servranckx, P. Webley, S. Barsotti, K. Dean, A. Durant, J. Ewert, A. Neri, W. Rose, et al. (2009), A multidisciplinary effort to assign realistic source parameters to models of volcanic ash-cloud transport and dispersion during eruptions, *Journal of Volcanology and Geothermal Research*, *186*(1), 10–21.

Noh, Y., W. Cheon, S.-Y. Hong, and S. Raash (2003), Improvement of the K-profile model for the planetary boundary layer based on large eddy simulation data, *Boundary Layer Meteorol.*, *107*, 401–427.

Palmer, T., and P. D. Williams (2008), Introduction. stochastic physics and climate modelling, *Philosophical Transactions of the Royal Society A: Mathematical, Physical and Engineering Sciences*, *366*(1875), 2419–2425.

Palmer, T., R. Buizza, F. Doblas-Reyes, T. Jung, M. Leutbecher, G. Shutts, M. Steinheimer, and A. Weisheimer (2009), *Stochastic parametrization and model uncertainty*, European Centre for Medium-Range Weather Forecasts.

Plant, R., and G. C. Craig (2008), A stochastic parameterization for deep convection based on equilibrium statistics, *Journal of the Atmospheric Sciences*, *65*(1), 87–105.

Potempski, S., S. Galmarini, R. Addis, P. Astrup, S. Bader, R. Bellasio, R. Bianconi, F. Bonnardot, R. Buckley, R. D'Amours, et al., Multi-model ensemble analysis of the etex-2 experiment, *Atmospheric Environment*, *42*(31), 7250–7265, 2008.

Pouget, S., M. Bursik, P. Webley, J. Dehn, and M. Pavolonis, Estimation of eruption source parameters from umbrella cloud or downwind plume growth rate, *Journal of Volcanology and Geothermal Research*, *258*, 100–112, 2013.

Raftery, A. E., D. Madigan, and J. A. Hoeting (1997), Bayesian model averaging for linear regression models, *Journal of the American Statistical Association*, *92*(437), 179–191.

Searcy, C., K. Dean, and B. Stringer (1998), PUFF: A high-resolution volcanic ash tracking model, *J. Volcanology and Geothermal Research*, *80*, 1–16.

Shutts, G. (2005), A kinetic energy backscatter algorithm for use in ensemble prediction systems, *Quarterly Journal of the Royal Meteorological Society*, *131*(612), 3079–3102.

Shutts, G. (2008), The forcing of large-scale waves in an explicit simulation of deep tropical convection, *Dynamics of Atmospheres and Oceans*, *45*(1), 1–25.

Skamarock, W., J. Klemp, J. Dudhia, D. Gill, D. Barker, W. Wang, and J. Powers (2005), A Description of the Advanced Research WRF Version 2.

Stohl, A., A. Prata, S. Eckhardt, L. Clarisse, A. Durant, S. Henne, N. Kristiansen, A. Minikin, U. Schumann, P. Seibert, et al., Determination of time-and height-resolved volcanic ash emissions and their use for quantitative ash dispersion modeling: the 2010 eyjafjallajökull eruption, *Atmospheric Chemistry and Physics*, *11*(9), 4333–4351, 2011.

Toth, Z., and E. Kalnay (1993), Ensemble forecasting at NMC: The generation of perturbations, *Bull. Amer. Meteor. Soc.*, *74*, 2317–2330.

UCAR (2012), Users Guide for the Advanced Research WRF (ARW) Modeling System Version 3.4, `http://www.mmm.ucar.edu/wrf/users/docs/user_guide_V3/contents.html`.

UWYO (2012), 03005 Lerwick Observations, `http://weather.uwyo.edu/upperair/sounding.html`.

Warner, T. T. (2011), *Numerical weather and climate prediction*, vol. 526, Cambridge University Press Cambridge.

Webley, P., T. Steensen, M. Stuefer, G. Grell, S. Freitas, and M. Pavolonis (2012), Analyzing the Eyjafjallajökull 2010 eruption using satellite remote sensing, lidar and WRF-Chem dispersion and tracking model, *Journal of Geophysical Research: Atmospheres (1984–2012)*, *117*(D13).

Wei, M., Z. Toth, R. Wobus, and Y. Zhu (2008), Initial perturbations based on the ensemble transform (ET) technique in the NCEP global operational forecast system, *Tellus*, *60A*, 60–79.

Zhang, Z., and T. Krishnamurti (1999), A perturbation method for hurricane ensemble predictions, *Monthly Weather Review*, *127*(4), 447–469.

Corresponding author: M. Bursik, Department of Geology, University at Buffalo, 411 Cooke Hall, Buffalo, NY 14260, USA. (mib@buffalo.edu)

Table 1. Combinations of WRF multi-model parameters. Microphysics: 1, Kessler; 4, 5-moment; 6, 6-moment. PBL: 2, Mellor-Yamada-Janjic; 4, Quasi-Normal Scale Elimination; 5, Niino Level 2.5. K: 1, Constant; 4, 2D deformation.

Microphysics	PBL	K
1	2	1
1	2	4
1	4	1
1	4	4
1	5	1
4	2	1
6	2	1

Table 2. Skills and measures compared for use of eruption source parameter against eruption source parameter + windfield uncertainty.

	Skills				Measures		
	Brier score	Reliability	Resolution	Uncertainty	RMSE	Pearson coeff	Dice coeff
eruption source parameter uncertainty only	0.3225	0.3216	5.617e-05	0.002537	0.5675316	-0.2020078	0.0148148
eruption source parameter + windfield uncertainty	0.2048	0.2036	3.881e-05	0.003253	0.4478977	-0.1550349	0.0164684

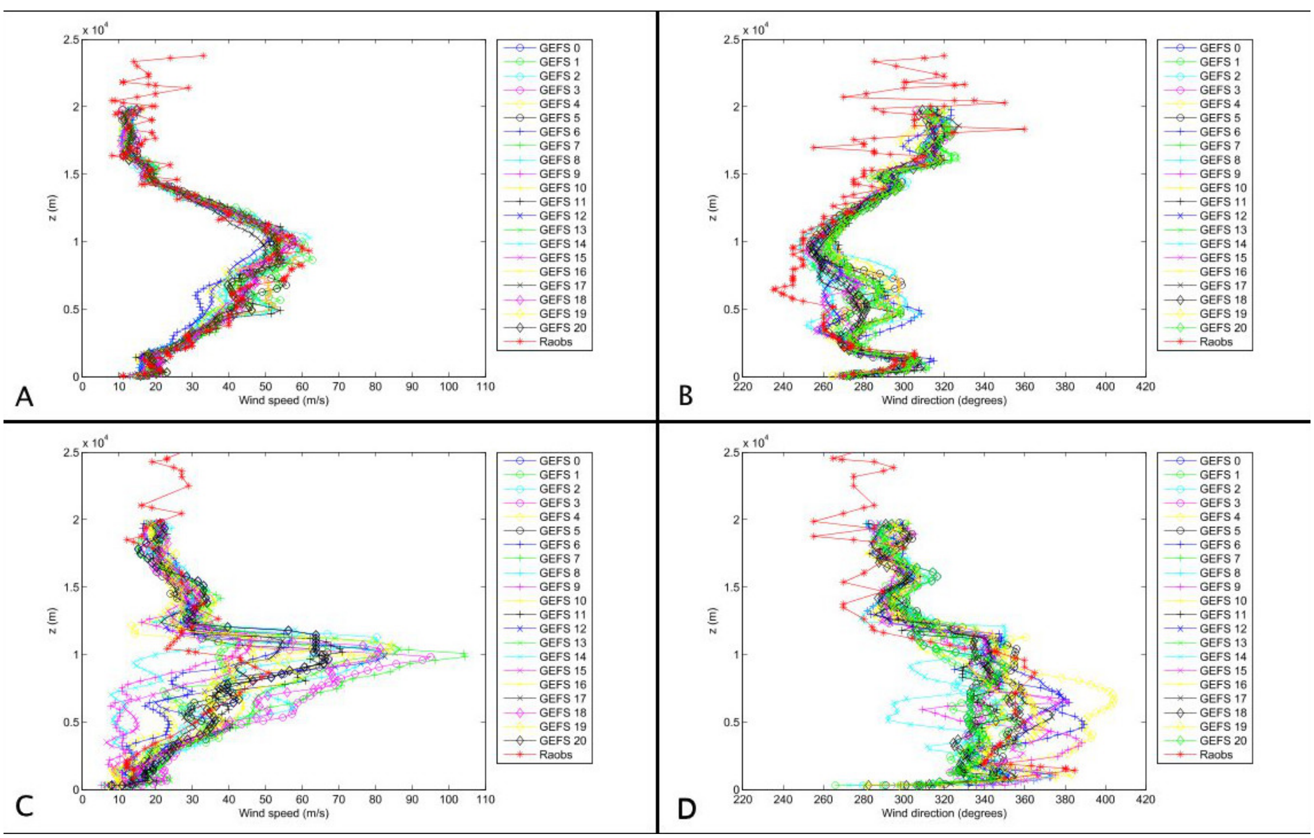

Figure 1. Comparison of wind speed (m/s) and wind direction (degrees) from radiosondes with those from GEFS and WRF multi-model output at (A and B), Praha station – 00h forecast (C and D), and with multiphysics output at Praha station – 72h forecast.

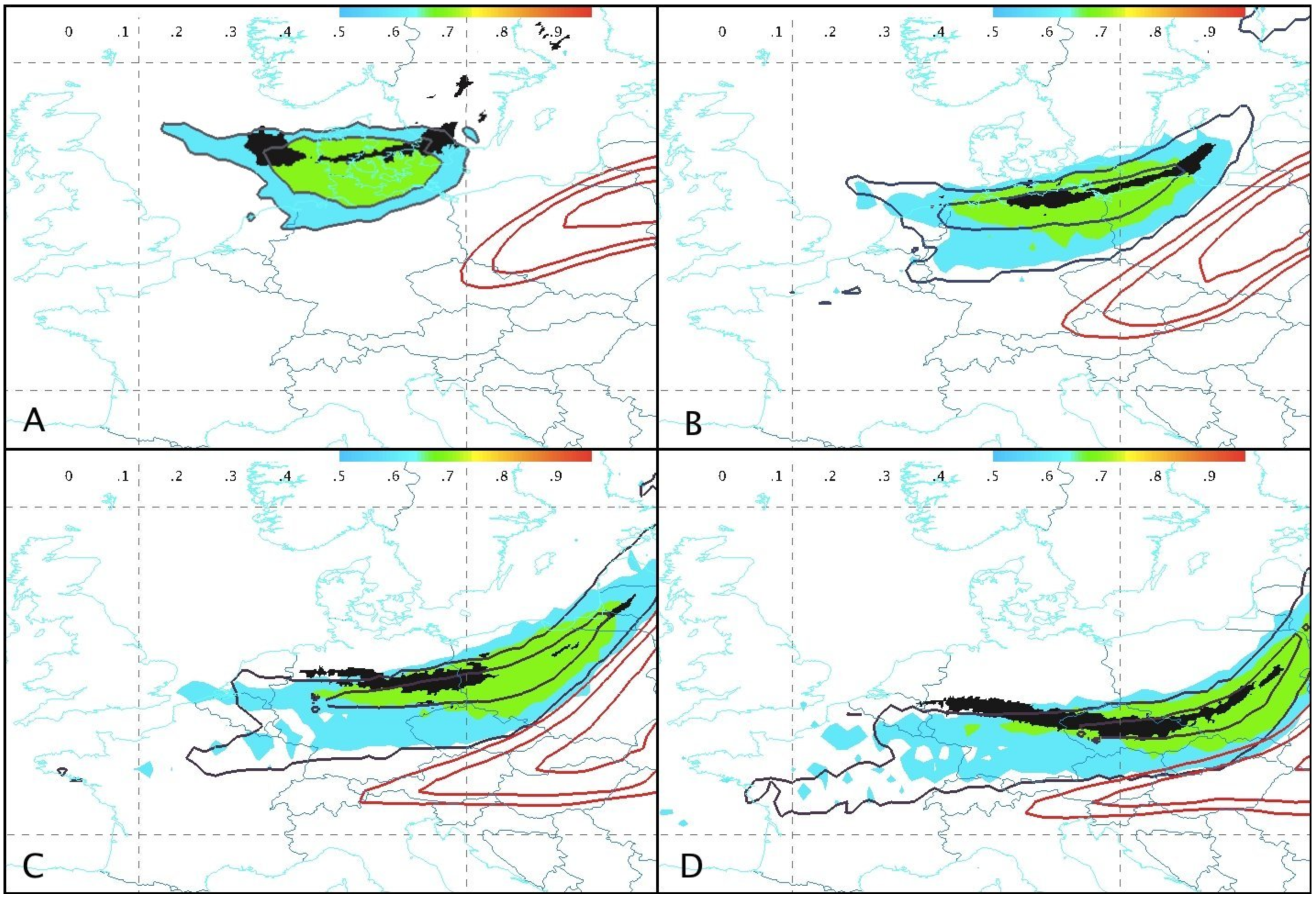

Figure 2. Average probability of having airborne ash when accounting for source parameters only (color fill); source parameters and wind field variability - forecast starting 0000 UTC April 16 (black probability contour); source parameters and wind field variability – forecast starting 0000 UTC April 14 (red probability contour), and corresponding satellite image (black fill), (A) 0000 UTC April 16, (B) 0006 UTC April 16, (C) 0012 UTC April 16, and (D) 0018 UTC April 16

.

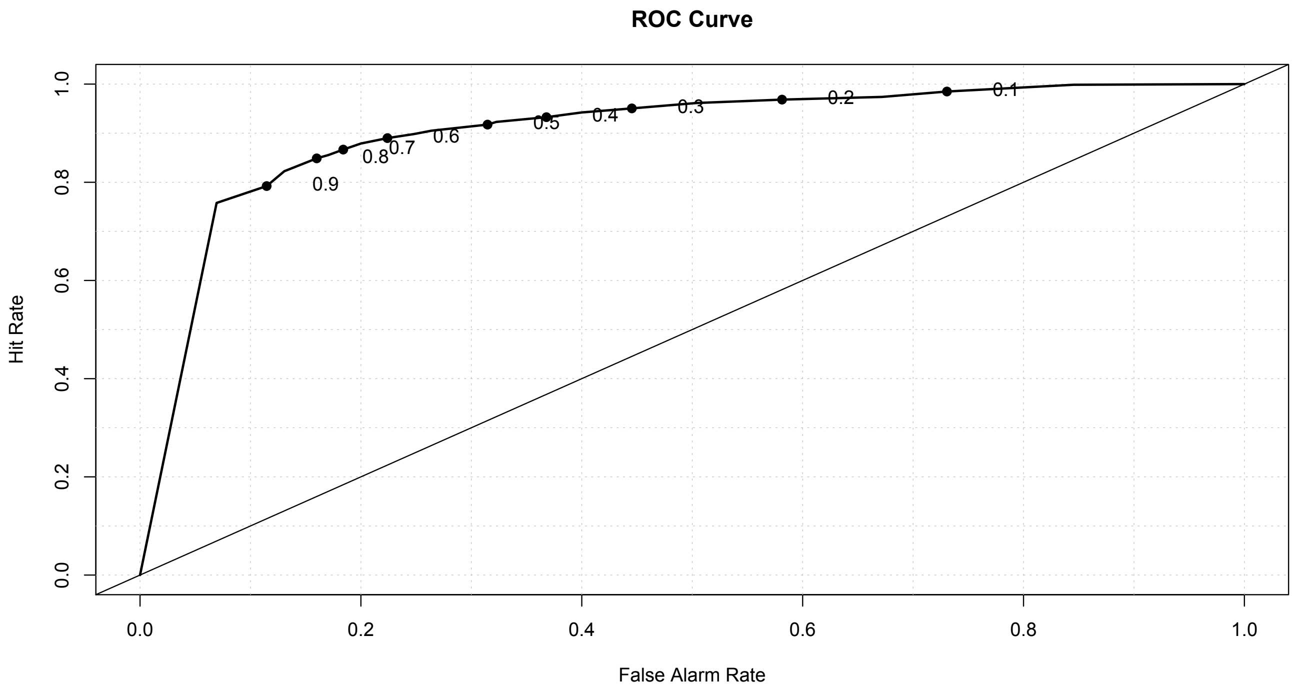

(a)

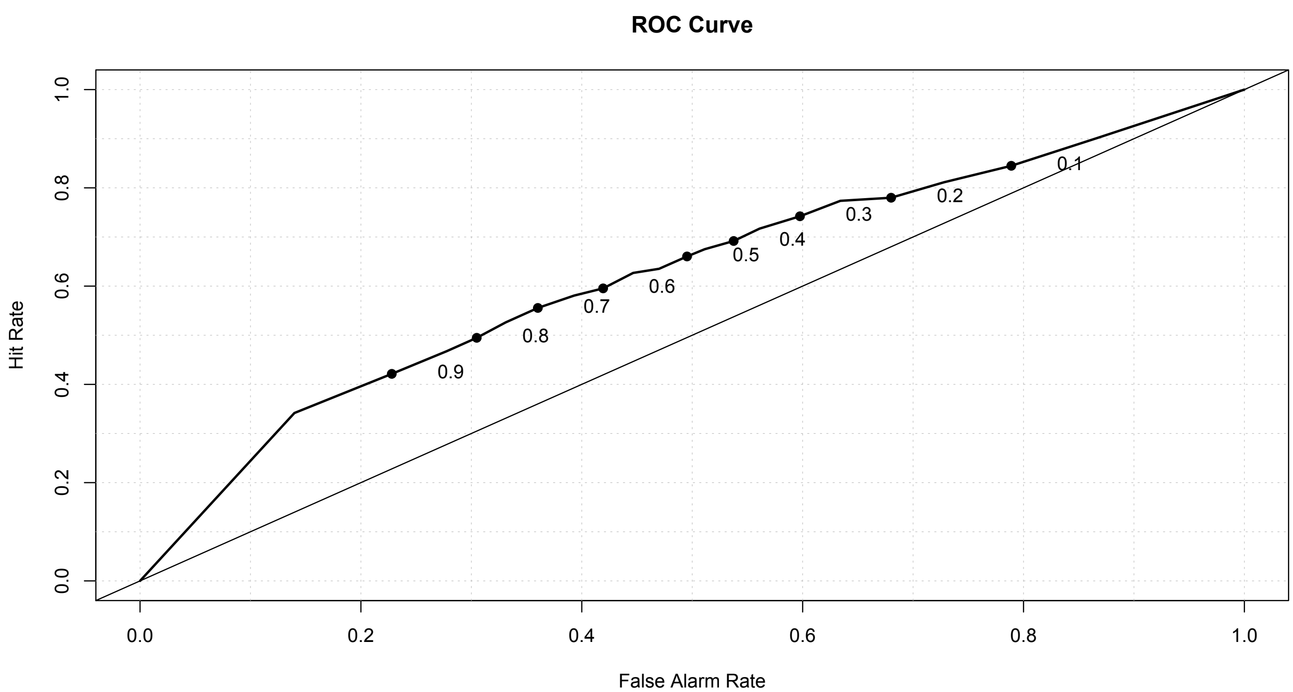

(b)

Figure 3. Receiver Operating Characteristics (ROC) for maximum height of concentration exceeding 10^{-10} for source parameters and wind field variability and source parameters only a) forecast starts 0006 UTC April 16 b) forecast start at 0006 UTC April 14.

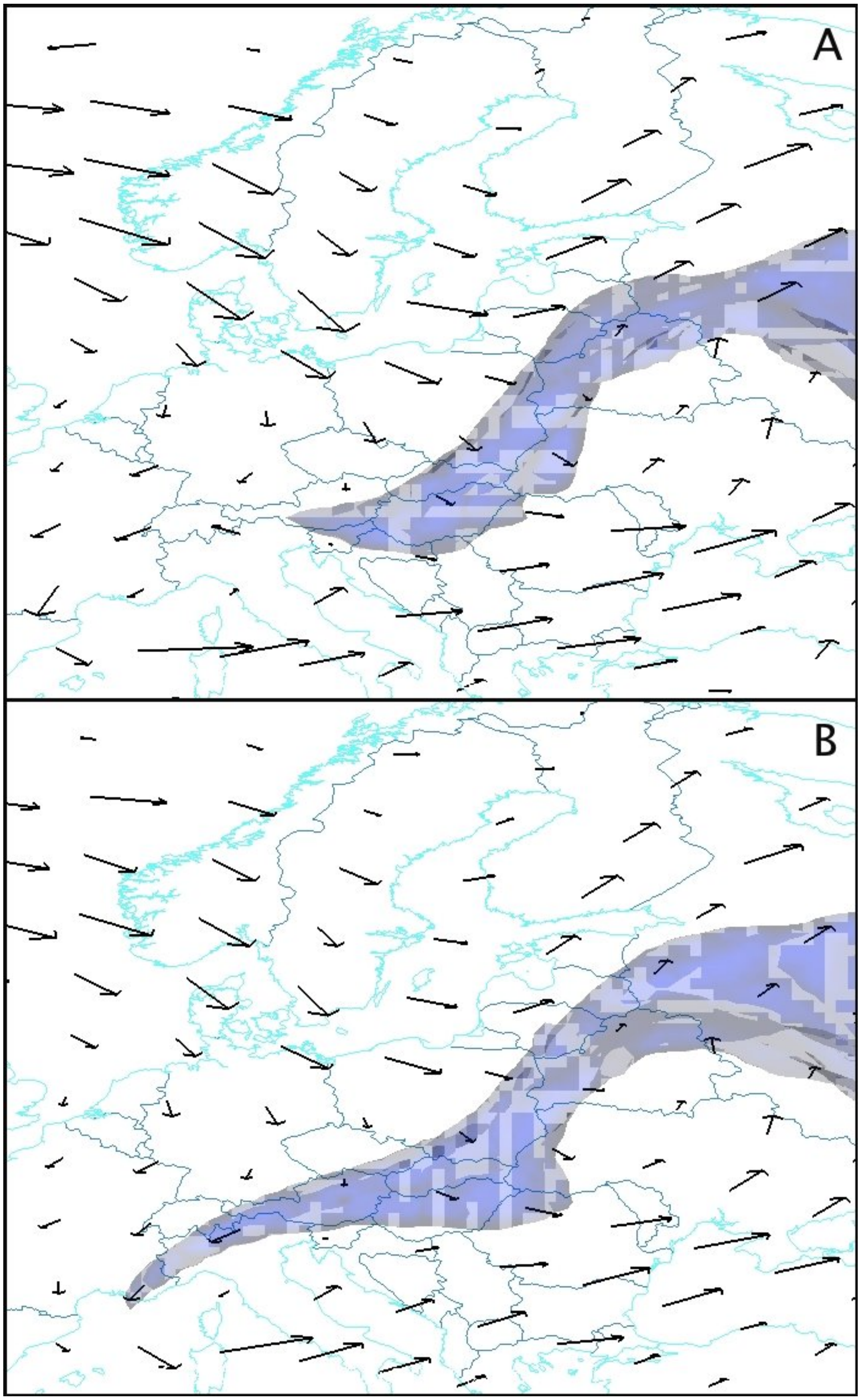

Figure 4. (a) The 0005 UTC April 14 forecast starting 0000 UTC April 16 compared to the